PROCEEDINGS OF THE ROYAL SOCIETY A

Proc. R. Soc. A (2007) **463**, 21–48
doi:10.1098/rspa.2006.1729
Published online 25 July 2006

The evolution of large ocean waves: the role of local and rapid spectral changes

By R. S. Gibson and C. Swan*

Department of Civil and Environmental Engineering, Imperial College London, London SW7 2AZ, UK

This paper concerns the formation of large-focused or near-focused waves in both unidirectional and directional sea-states. When the crests of wave components of varying frequency superimpose at one point in space and time, a large, transient, focused wave can occur. These events are believed to be representative of the largest waves arising in a random sea and, as such, are of importance to the design of marine structures. The details of how such waves form also offer an explanation for the formation of the so-called *freak* or *rogue* waves in deep water. The physical mechanisms that govern the evolution of focused waves have been investigated by applying both the fully nonlinear wave model of Bateman *et al.* (Bateman *et al.* 2001 *J. Comput. Phys.* **174**, 277–305) and the Zakharov's evolution equation (Zakharov 1968 *J. Appl. Mech. Tech. Phys.* **9**, 190–194). Aspects of these two wave models are complementary, and their combined use allows the full nonlinearity to be considered and, at the same time, provides insights into the dominant physical processes.

In unidirectional seas, it has been shown that the local evolution of the wave spectrum leads to larger maximum crest elevations. In contrast, in directional seas, the maximum crest elevation is well predicted by a second-order theory based on the underlying spectrum, but the shape of the largest wave is not. The differences between the evolution of large waves in unidirectional and directional sea-states have been investigated by analysing the results of Bateman *et al.* (2001) using a number of spectral analysis techniques. It has been shown that during the formation of a focused wave event, there are significant and rapid changes to the underlying wave spectrum. These changes alter both the amplitude of the wave components and their dispersive properties. Importantly, in unidirectional sea-states, the bandwidth of the spectrum typically increases; whereas, in directional sea-states it decreases.

The changes to the wave spectra have been investigated using Zakharov's equation (1968). This has shown that the third-order *resonant* effects dominate changes to both the amplitude of the wave components and the dispersive properties of the wave group. While this is the case in both unidirectional and directional sea-states, the consequences are very different. By examining these consequences, directional sea-states in which large wave events that are higher and steeper than second-order theory would predict have been identified. This has implications for the types of sea-states in which *rogue* waves are most likely to occur.

Keywords: surface-water waves; focused waves; nonlinear waves; directional waves; rogue waves; resonant interactions

* Author for correspondence (c.swan@imperial.ac.uk).

The electronic supplementary material is available at http://dx.doi.org/10.1098/rspa.2006.1729 or via http://www.journals.royalsoc.ac.uk.

Received 11 April 2005
Accepted 3 April 2006

1. Introduction

The water surface of a realistic ocean environment can be described by the sum of wave components, of different frequency, travelling in different directions. If the crests of the wave components come into phase at one point in space and time, they superimpose to form a large focused wave event. Such waves are believed to be representative of the largest waves in a sea-state. The details of how large waves form is of the utmost importance to the design of marine vessels and structures. For shipping, the assessment of extreme crest elevations is critical in determining the applied loads, vessel response, occurrence of green-water inundation and incidences of wave slamming. Whereas, in the design of a fixed structure, the deck elevation is traditionally set to maintain an effective air gap, so even the highest crest elevations do not impact on the underside of the structure. Furthermore, the focusing of wave components offers a possible explanation for the occurrence of *freak* or *rogue* waves; describing those events, which are higher or occur more often than is statistically predicted. Indeed, a large focused wave crest has all the characteristics of a *freak* wave, it is transient, appearing almost out of nowhere, has large crest–trough asymmetry and during its formation, significant and rapid nonlinear interactions can occur that increase both the crest elevation and the wave steepness.

Building on the work of Lindgren (1970) and Boccotti (1983), the new wave theory of Tromans *et al.* (1991) predicts that, according to linear theory, a focused wave profile, corresponding to the scaled autocorrelation of the underlying spectrum, is the most probable shape of the highest waves. If second-order nonlinearities are accounted for, the analysis of field measurements by Jonathan *et al.* (1994) indicate that this is indeed the case. However, the nonlinearity of a large transient wave event is not restricted to second order; there are not only higher-order *bound* nonlinearities, but at third order and above, there are also *resonant* nonlinearities. For a regular wave, the *bound* nonlinearities are the higher-order terms derived by Stokes (1847), and are represented by bound waves that are phase locked to the underlying linear wave component. Similarly, in an irregular wave field, they can be described to second order by the theory of Sharma & Dean (1981). In both cases, the *bound* nonlinearities alter the shape of a wave profile by sharpening the peaks and broadening the troughs.

In contrast, the *resonant* nonlinearities lead to the redistribution of energy within a wave spectrum, and can thus alter the amplitude and phase of the underlying linear wave components. The transfer of energy was first studied in relation to pairs of wave components by Phillips (1960), with interactions identified as *resonant* since they had the mathematical form of a linear resonator. A *resonant* interaction occurs when the interaction between wave components satisfies the dispersion relationship. When this occurs, the interaction between these components forces a wave mode that can propagate freely and energy is exchanged between the various components. The conditions, in deep water, under which this can occur are expressed as

$$k_i = \sum_j^N s_j k_j, \tag{1.1a}$$

$$\omega_i = \sum_j^N s_j \omega_j, \tag{1.1b}$$

$$\omega_i^2 = g k_i, \tag{1.1c}$$

$$s_j = \pm 1, \tag{1.1d}$$

where k is the wavenumber, ω the wave frequency and the subscript i identifies the wave component that is being forced. For deep-water gravity waves, this condition can only be met for $N \geq 3$, and hence, can only occur at third and higher order. These nonlinearities account for both the instability of a regular wave in a laboratory flume (Benjamin & Feir 1967) and the long-term evolution of a wave spectrum (Hasselmann 1962). However, the former is often described as a case of *near resonance*, as the condition expressed by equation (1.1*b*) is not met exactly owing to *resonant* changes in the frequency of the wave components; this is discussed further in §5. Moreover, in relation to extreme crest elevations, evidence discussed in §2 suggests that during the formation of a focused wave event, the *resonant* (and in particular the *near resonant*) interactions can occur extremely rapidly. This can lead to the wave profile becoming much higher and steeper than would be expected from the predictions of linear or second-order theory.

In the current paper, the formation of focused wave events will be investigated by applying two, very different, nonlinear wave models. These will be described in §3 and the significance of the *bound* and *resonant* nonlinearities ascertained for a number of realistic wave fields. It will be shown that the evolution of wave spectra is fundamental to the formation of the largest wave events. This will be described in §4. In §5, the physical mechanisms responsible for this evolution will be ascertained. Finally, §6 provides some concluding remarks and discusses the practical implications.

2. Background

Baldock *et al.* (1996) measured the water surface profile and the water particle kinematics associated with a number of unidirectional-focused wave events in a laboratory flume. They found that the measured crest elevations were typically of the order of 35% higher than the linear prediction and 25% higher than the second-order prediction. One of the wave cases that they investigated was a narrow-banded spectrum with wave components of equal amplitude, uniformly distributed within the period range $0.8 < T < 1.2$ s. By examining the spectrum measured at the location of the extreme crest, they were able to identify significant energy lying within the range $0.6 < T < 0.8$ s. This could not be attributed to either the linear input or the second-order nonlinearities. Hence, they argued that it represented a local and rapid widening of the underlying linear spectrum and it was responsible for the large increase in maximum crest elevation. Johannessen & Swan (2001) extended this work by examining directionally spread focused wave events. They found that as the sea-state became more short crested, second-order theory rapidly became sufficient to predict the maximum crest elevation. Both of these experimental investigations highlight the importance of considering both the full nonlinearity and the directionality of a sea-state when describing extreme transient waves. The transfer of energy during the formation of an extreme wave event was investigated further by Johannessen & Swan (2003) with the use of a fully nonlinear numerical directional wave model, based upon the unidirectional formulation of Fenton & Rienecker (1982). By using a numerical wave model, they were able to generate data with a much higher spatial resolution than is possible in the laboratory. The analysis of this data led to spectra in both wavenumber and wave frequency. As a result, they were able to identify a rapid transfer of energy to high wavenumbers that appeared to be freely propagating, but did not quite satisfy the linear dispersion relationship. Furthermore, by incorporating the evolved spectrum of freely propagating wave components into the second-order theory of Sharma & Dean (1981), they were able to predict both the extreme crest elevation and the water particle kinematics with good accuracy. However, Johannessen & Swan (2003) were not able to identify the physical mechanisms responsible for this transfer of energy. Furthermore, the numerical wave model was restricted to modelling unrealistic narrow-banded spectra of the type used in the laboratory experiments of Baldock *et al.* (1996) and Johannessen & Swan (2001).

3. Two nonlinear wave models

To investigate the fully nonlinear evolution of a realistic, broad-banded, directionally spread sea-state, it is necessary to use a fully nonlinear wave model that can incorporate all of these features. Furthermore, in order to understand the fully nonlinear results, it is desirable to use a wave model that isolates the contributions from the various physical processes. This section describes two nonlinear wave models. The first is that of Bateman *et al.* (2001), hereafter known as BST. This is a fully nonlinear numerical wave model that can accurately and efficiently model the evolution of realistic, directionally spread, wave spectra. The second model is based on Zakharov's equation (Zakharov 1968) hereafter known as ZE. This is a nonlinear evolution equation that can be applied to realistic, directionally spread, wave spectra and has been derived in Hamiltonian form up to fourth order by Krasitskii (1994). Although the two wave models have a number of important similarities, the ordering of the terms within their representative series solutions is fundamentally different. BST adopts a Fourier series representation in which individual wave components can be isolated, but their physical properties and, perhaps more importantly, their physical origins remain uncertain. In particular, it is difficult within the BST model to determine whether a wave component is bound or freely propagating, and from which wave interactions a wave component arises. In fact, each wave component may well represent a number of different free and bound waves and arise from a combination of different interactions. However, provided the model includes a sufficiently large number of wave components, the numerical results may be considered fully nonlinear. In contrast, the model referred to as ZE is based upon the Krasitskii (1994) fourth-order formulation. Although this is limited in terms of nonlinearity, it clearly identifies the physical properties of the evolving wave components, and the wave interactions from which they have arisen. By utilizing both models, it is possible to ensure that the full nonlinearity has been addressed and to gain some understanding as to the physical processes that are responsible for the results obtained.

(*a*) *Description of the wave models*

BST developed a numerical three-dimensional wave model based upon the unidirectional formulation of Craig & Sulem (1993); the equation set on which these models are based having been considered earlier by Milder (1977) and Stiassnie & Shemer (1984). In the present paper, the relevant model results are noted as BST, since this describes the actual model employed and provides a first account of how directionality may be included. Within this model, the water surface profile and the velocity potential on the surface are described by Fourier series and are time-marched as suggested by Zakharov (1968). The efficiency of the model relies upon the calculation of the spatial derivatives of the potential on the surface by applying a Dirichlet–Neumann operator. The application of this operator leads to a procedure that is many times more efficient than one based upon large matrix inversion (e.g. Fenton & Rienecker 1982). As a result, the wave model is able to incorporate a very large range of length-scales and is therefore capable of accurately modelling the evolution of realistic broad-banded directionally spread sea-states containing near-breaking waves. It has been shown to be in excellent agreement with both the laboratory data of Johannessen & Swan (2001) and the numerical results of Johannessen & Swan (2003). A detailed account of its application can be found in Bateman & Swan (submitted). However, while the results are exact, accounting for the full nonlinearity, they give very little direct indication as to the physical processes controlling the evolution.

Zakharov's equation is an integro-differential equation that can describe the evolution of a broad-banded directionally spread sea-state. Although it has only been derived to fourth order, the ability to isolate the various wave interactions allows the physical processes, controlling the formation of an extreme wave event to be identified. A complete derivation can be found in Krasitskii (1994), the manner in which it can be applied numerically is described in Annenkov & Shrira (2001), and the effect of discretization studied by Rasmussen & Stiassnie (1999). Furthermore, it has been shown by Shemer *et al.* (2001) to be in good qualitative agreement with laboratory data concerning the evolution of both a bimodal and a Gaussian spectrum. An explanation of ZE, following the derivation of Krasitskii (1994), is given below; the main purpose of which is to highlight the physical significance of the various terms and to clarify the advantages of using the model.

The evolution of wave motion can be described (Zakharov 1968) in Hamiltonian form as follows:

$$\frac{\partial\eta(x,t)}{\partial t}=\frac{\delta H}{\delta\varphi(x,t)},\quad \frac{\partial\varphi(x,t)}{\partial t}=-\frac{\delta H}{\delta\eta(x,t)}, \tag{3.1}$$

where δ are functional derivatives and the Hamiltonian, H, is the sum of the potential and kinetic energy. The surface profile, $\eta(\boldsymbol{x})$, and the value of the velocity potential on the surface $\varphi(\boldsymbol{x})$, are described in terms of their Fourier integrals $\eta(\boldsymbol{k})$ and $\varphi(\boldsymbol{k})$, respectively,

$$\left.\begin{aligned}\varphi(\boldsymbol{x})&=\frac{1}{2\pi}\int_{-\infty}^{\infty}\varphi(\boldsymbol{k})\mathrm{e}^{\mathrm{i}\boldsymbol{k}\cdot\boldsymbol{x}}\,\mathrm{d}\boldsymbol{k},\\ \eta(\boldsymbol{x})&=\frac{1}{2\pi}\int_{-\infty}^{\infty}\eta(\boldsymbol{k})\mathrm{e}^{\mathrm{i}\boldsymbol{k}\cdot\boldsymbol{x}}\,\mathrm{d}\boldsymbol{k},\end{aligned}\right\} \tag{3.2}$$

where $\boldsymbol{x}$ is the spatial coordinate and $\boldsymbol{k}$ is the wavenumber vector. These are transformed into a pair of canonical conjugate variables $a(\boldsymbol{k})$ and $ia^*(\boldsymbol{k})$, such that

$$i\frac{\partial a(\boldsymbol{k})}{\partial t} = \frac{\delta H}{\delta a^*(\boldsymbol{k})}, \tag{3.3}$$

$$\eta(\boldsymbol{k}) = M(\boldsymbol{k})[a(\boldsymbol{k}) + a^*(-\boldsymbol{k})], \tag{3.4a}$$

$$\varphi(\boldsymbol{k}) = -iN(\boldsymbol{k})[a(\boldsymbol{k}) - a^*(-\boldsymbol{k})], \tag{3.4b}$$

$$M(\boldsymbol{k}) = \left[\frac{\boldsymbol{q}(\boldsymbol{k})}{2\omega(\boldsymbol{k})}\right]^{1/2}, \tag{3.4c}$$

$$N(\boldsymbol{k}) = \left[\frac{\omega(\boldsymbol{k})}{2\boldsymbol{q}(\boldsymbol{k})}\right]^{1/2}, \tag{3.4d}$$

where $\boldsymbol{q}(\boldsymbol{k}) = |\boldsymbol{k}|\tanh(|\boldsymbol{k}|d)$, d is the water depth and $\omega(\boldsymbol{k}) = \sqrt{g\boldsymbol{q}(\boldsymbol{k})}$; the latter defining the linear dispersion relationship.

With the Hamiltonian H, expanded as an integral power series in a, the evolution equation for a (from equations (3.1)) has been derived to fourth order by Krasitskii (1994), but is expressed below to third order,

$$\begin{aligned} i\frac{\partial a_0}{\partial t} = \frac{\partial \mathbf{H}}{\partial a_0^*} = \omega_0 a_0 &+ \iint U^{(1)}_{0,1,2} a_1 a_2 \boldsymbol{\Delta}_{0-1-2}\, \mathrm{d}k_1\, \mathrm{d}k_2 \\ &+ \iint U^{(2)}_{0,1,2} a_1^* a_2 \boldsymbol{\Delta}_{0+1-2}\, \mathrm{d}k_1\, \mathrm{d}k_2 \\ &+ \iint U^{(3)}_{0,1,2} a_1^* a_2^* \boldsymbol{\Delta}_{0+1+2}\, \mathrm{d}k_1\, \mathrm{d}k_2 \\ &+ \iiint V^{(1)}_{0,1,2,3} a_1 a_2 a_3 \boldsymbol{\Delta}_{0-1-2-3}\, \mathrm{d}k_1\, \mathrm{d}k_2\, \mathrm{d}k_3 \\ &+ \iiint V^{(2)}_{0,1,2,3} a_1^* a_2 a_3 \boldsymbol{\Delta}_{0+1-2-3}\, \mathrm{d}k_1\, \mathrm{d}k_2\, \mathrm{d}k_3 + \cdots, \end{aligned} \tag{3.5}$$

where a_0 is the wave component that is evolving, $\boldsymbol{\Delta}_{a,b,c}$ is shorthand for the delta-function which equals 1 if $k_a + k_b + k_c = 0$ and zero otherwise, and the kernels $U^{(1)}$, $U^{(2)}$, $U^{(3)}$, $V^{(1)}$ and $V^{(2)}$ are known functions of wavenumber and water depth. This integral power series consists of both *bound* interactions, that do not alter the underlying linear spectrum and *resonant* interactions that do. For example, the integrals involving the $U^{(i)}$ kernels are equivalent to the second-order *bound* interactions calculated by Sharma & Dean (1981); while the integrals involving the $V^{(i)}$ kernels define both third-order *bound* and *resonant* interactions. Equation (3.5) could be time marched to model the evolution of the spectrum. This would include both the *bound* and the *resonant* interactions. However, as it is only the *resonant* interactions that alter the underlying spectrum, it is possible to reduce this equation by the transforming the variables $a(\boldsymbol{k})$ and $ia^*(\boldsymbol{k})$ to the canonically conjugate variables $b(\boldsymbol{k})$ and $ib^*(\boldsymbol{k})$,

$$\begin{aligned} a_0 = b_0 &+ \iint A^{(1)}_{0,1,2} b_1 b_2 \Delta_{0-1-2}\, \mathrm{d}k_1\, \mathrm{d}k_2 \\ &+ \iint A^{(2)}_{0,1,2} b_1^* b_2 \Delta_{0+1-2}\, \mathrm{d}k_1\, \mathrm{d}k_2 \\ &+ \iint A^{(3)}_{0,1,2} b_1^* b_2^* \Delta_{0+1+2}\, \mathrm{d}k_1\, \mathrm{d}k_2 \\ &+ \iiint B^{(1)}_{0,1,2,3} b_1 b_2 b_3 \Delta_{0-1-2-3}\, \mathrm{d}k_1\, \mathrm{d}k_2\, \mathrm{d}k_3 + \cdots. \end{aligned} \tag{3.6}$$

The various kernels A and B are now exclusively the *bound* interactions, and hence, the evolution of the underlying linear wave components can be expressed entirely in terms of the *resonant* interactions (expressed below to fourth order)

$$\begin{aligned} i\frac{\partial B_m}{\partial t} = &\sum_{n=1}^{N}\sum_{p=1}^{N}\sum_{q=1}^{N} \tilde{V}^{(2)}_{m,n,p,q} B_n^* B_p B_q\, \mathrm{e}^{\mathrm{i}(\omega_m+\omega_n-\omega_p-\omega_q)t}\, \Delta_{m+n-p-q} \\ &+ \sum_{n=1}^{N}\sum_{p=1}^{N}\sum_{q=1}^{N}\sum_{r=1}^{N} \tilde{W}^{(2)}_{m,n,p,q,r} B_n^* B_p B_q B_r\, \mathrm{e}^{\mathrm{i}(\omega_m+\omega_n-\omega_p-\omega_q-\omega_r)t}\, \Delta_{m+n-p-q-r} \\ &+ \sum_{n=1}^{N}\sum_{p=1}^{N}\sum_{q=1}^{N}\sum_{r=1}^{N} \tilde{W}^{(3)}_{m,n,p,q,r} B_n^* B_p^* B_q B_r\, \mathrm{e}^{\mathrm{i}(\omega_m+\omega_n+\omega_p-\omega_q-\omega_r)t}\, \Delta_{m+n+p-q-r}, \end{aligned} \tag{3.7}$$

where $B(\boldsymbol{k}, t) = b(\boldsymbol{k}, t)\mathrm{e}^{\mathrm{i}\omega(\boldsymbol{k})t}$.

Equation (3.7) describes the evolution of an underlying linear wave component in terms of third-order resonant interactions, $\tilde{V}$, and fourth-order resonant interaction, $\tilde{W}$. It can be time marched using a standard Runge–Kutta algorithm and then the surface profile recreated at each time-step to the desired order by re-incorporating the *bound* interactions of equation (3.6). However, the essential benefit of this approach is that it is possible to choose which interactions are included and which are neglected, and hence to isolate the physical processes (or wave interactions) that control the evolution of the wave field.

During the review process, important questions were raised concerning the validity of the comparison between the two wave models; specifically whether the transformation noted above may be a source of distortions in the Fourier spectrum of the solutions. To allay such fears, electronic supplementary material has been added in which the Krasitskii implementation of Zakharov's equation is shown to exactly reproduce three well-known nonlinear wave effects. These are the nonlinear changes in a regular wave form; the interactions arising at second order when two wave components coexist (Longuet-Higgins & Stewart 1960); and the third-order changes in the phase arising when two wave components interact (Longuet-Higgins & Phillips 1962). Using these results, the renormalization necessary to ensure consistent comparisons between the two wave models (BST and ZE) is further discussed.

Table 1. Details of the wave spectra, investigated. The four cases highlighted are those considered in detail in this paper. The parameters are defined as follows: for the laboratory-scale Top-hat spectra, the total amplitude of the spectrum is spread evenly in period, T, between $T_L < T < T_U$; for the JONSWAP spectrum, T_p is the peak period, γ the peak-enhancement factor and σ_s the standard deviation of the wrapped-normal directional spreading function (all other parameters, $\alpha = 0.0081$ and $\beta = 1.25$, are held constant for these cases); and for the Gaussian spectra, T_p is the mean period, σ_g the standard deviation in the period domain and σ_s as before.

		parameters					
case	spectral form	T_L (s)	T_U (s)	T_p (s)	γ	σ_s	σ_g
NB	**Top-hat**	**0.8**	**1.2**	**n.a.**	**n.a.**	**0**	**n.a.**
BB	Top-hat	0.6	1.4	n.a.	n.a.	0	n.a.
J1D0	JONSWAP	n.a.	n.a.	12.8	1	0	n.a.
J5D0	**JONSWAP**	**n.a.**	**n.a.**	**12.8**	**5**	**0**	**n.a.**
J1D5	JONSWAP	n.a.	n.a.	12.8	1	5	n.a.
J1D10	JONSWAP	n.a.	n.a.	12.8	1	10	n.a.
J1D30	JONSWAP	n.a.	n.a.	12.8	1	30	n.a.
J5D5	**JONSWAP**	**n.a.**	**n.a.**	**12.8**	**5**	**5**	**n.a.**
J5D10	JONSWAP	n.a.	n.a.	12.8	5	10	n.a.
J5D30	**JONSWAP**	**n.a.**	**n.a.**	**12.8**	**5**	**30**	**n.a.**
J5D30T10	JONSWAP	n.a.	n.a.	10	5	30	n.a.
J5D30T16	JONSWAP	n.a.	n.a.	16	5	30	n.a.
G16D0	Gaussian	n.a.	n.a.	16	n.a.	0	2
G18D0	Gaussian	n.a.	n.a.	18	n.a.	0	2
G16D5	Gaussian	n.a.	n.a.	16	n.a.	5	2
G18D5	Gaussian	n.a.	n.a.	18	n.a.	5	2

(*b*) *Focused wave events*

The two wave models have been applied to study the formation of large focused wave events, in which the waves are at, or close to, their breaking limit. They are initiated with a desired amplitude spectrum, and the subsequent evolution of both the wave spectrum and the surface profile ascertained. Within the present study, a large number of focused waves arising in a variety of wave spectra have been considered, full details of which are given in table 1. However, the majority of the results presented herein concern four specific test cases: case NB, a laboratory scale spectrum used by both Baldock *et al.* (1996) and Johannessen & Swan (2001); case J5D0, a unidirectional JONSWAP spectrum; case J5D5, a long-crested JONSWAP spectrum; and case J5D30, a short-crested JONSWAP spectrum. The notation used to define the JONSWAP spectra is $\boldsymbol{JXDY}$, where the $\boldsymbol{X}$ refers to the peak-enhancement factor γ and $\boldsymbol{Y}$ is the standard deviation of the wrapped normal directional spreading function.

In each case, BST has been initiated with a dispersed sea-state at a point in time, t_0, well before the focused wave event occurs. The surface profile and the velocity potential are calculated using linear (or second-order) wave theory, and are time marched up to and beyond the extreme event. The spatial profile at the time of the highest wave is identified. In these cases, the phase of each component was selected at t_0 so that according to linear theory a perfectly focused (all the wave components

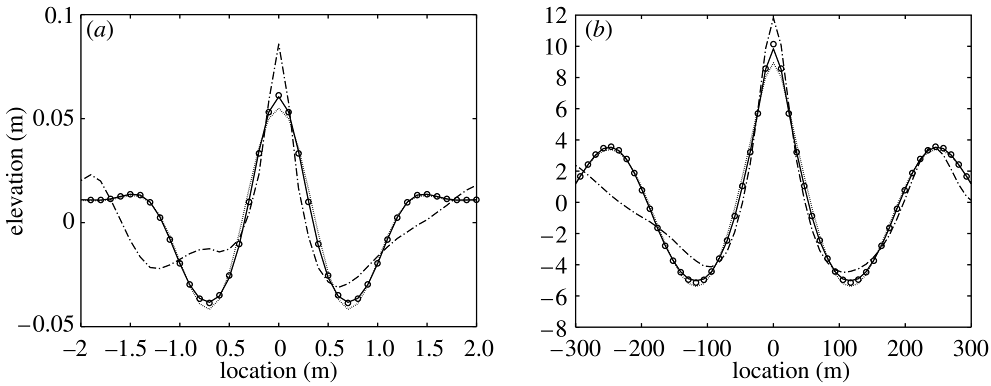

Figure 1. Surface profiles of two extreme wave events in unidirectional sea-states; comparisons between fully nonlinear calculations based on BST and *bound* wave solutions. (*a*) Case NB, (*b*) case J5D0. Dotted line, linear; solid line, second order; open circle, third order; dash-dotted line, fully nonlinear.

are exactly in phase) wave event would occur at $t=0$ s. However, the results confirm that not only do these events occur earlier than would be predicted, but they are not perfectly focused. Therefore, it might be expected that a change in the relative phasing of the wave components at t_0 will give an even greater fully nonlinear crest elevation. In unidirectional sea-states this is the case, however, the situation in directional sea-states is more complicated; an issue that is discussed in relation to the focal quality of the extreme event in §6.

The wave profile can be compared to the predictions based solely on *bound*-wave solutions: the linear solution based upon the superposition of Airy (1845) wave components; the second-order solution of Sharma & Dean (1981) (equivalent to utilizing the A kernels of equation (3.6)); and the third-order *bound* wave solution recovered by utilizing both the A and the B kernels of equation (3.6). The predictions based on the different orders of nonlinearity for the unidirectional cases NB and J5D0 are compared in figure 1. The location at which the crest occurs in the fully nonlinear simulations has been shifted in order to facilitate this comparison. It is clear that in both cases, the wave profile calculated using BST (fully nonlinear) is much higher and steeper than that predicted to linear (NB 56%, J5D0 34%), second (NB 42%, J5D0 22%) or even third order (NB 41%, J5D0 18%). Furthermore, the maximum crest elevation calculated to third order is only marginally (less than 4%) greater than that predicted to second order. This suggests that the inclusion of even higher-order *bound* interactions will not explain the difference between the fully nonlinear results and those of a *bound*-wave solution.

In contrast, figure 2 shows the profiles of the focused wave events in the directional seas, J5D5 and J5D30. Unlike the unidirectional cases, it has not been necessary to shift the location at which the crest occurs. While the maximum crest elevation is very similar to that predicted using a second-order bound-wave solution, the troughs associated with the highest wave are significantly shallower. Furthermore, in case J5D5, the extreme wave event occurs earlier than would be predicted. The results presented in figures 1 and 2 confirm that the formation of an extreme wave event cannot be predicted by simply applying a wave model that includes only the *bound* nonlinearities. Indeed, during the formation of an extreme

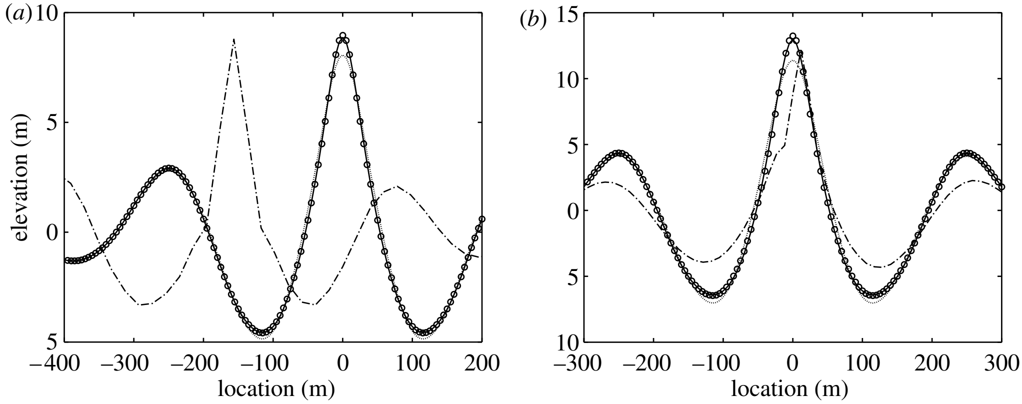

Figure 2. Surface profiles of two extreme wave events in directional sea-states; comparisons between fully nonlinear calculations based on BST and *bound* wave solutions. (*a*) Case J5D5, (*b*) case J5D30. Dotted line, linear; solid line, second order; open circle, third order; dash-dotted line, fully nonlinear.

wave event *resonant* interactions may be significant, and important physical processes can occur that result in the evolution of the wave spectrum. This evolution can lead to both significant increases in the maximum elevation associated with the largest waves and also to changes in their profile. By examining the details of this evolution in §4, and the physical mechanisms by which it occurs in §5, the fundamental differences between unidirectional and directional sea-states will be highlighted. This will enable situations in which extreme wave events in directional sea-states that are higher than would be predicted by a *bound*-wave solution to be ascertained. As a result, realistic sea-states in which *rogue* waves are intrinsically more likely to occur can be identified.

4. The movement of energy within a spectrum

In §4*a*, the results of BST will be analysed in order to describe the evolution of the wave spectrum during the formation of an extreme wave event. It is this evolution that is believed to be responsible for the failure of *bound*-wave solutions in predicting the shape of an extreme wave profile (figures 1 and 2). The results of BST will be analysed using two methods: the Fourier transform and the Stockwell transform (ST).

(*a*) *Two methods of spectral analysis*

The Fourier transform (equation (4.1)) is widely used in oceanography to generate wave spectra from measured surface records. With the use of the fast Fourier transform technique (FFT; Frigo & Johnson 1998), it is an extremely rapid and simple method of decomposing a surface trace in time (or space) into its frequency (or wavenumber) content:

$$X(f) = \int_{-\infty}^{\infty} x(t)\mathrm{e}^{(-\mathrm{i}2\pi ft)}\,\mathrm{d}t, \tag{4.1}$$

where $x(t)$ describes the magnitude of a variable (e.g. the elevation of the water surface) in time, and $X(f)$ is its Fourier transform, and hence, describes the frequency content of the record. However, the Fourier transform has one significant limitation, it assumes that the spectral content of a wave profile is stationary. As a result, any non-stationarity is modelled by the inclusion of harmonics that appear as a spread of energy that has no obvious physical meaning. Despite this, the Fourier transform has been applied to the surface profile, $\eta(\boldsymbol{x})$, at different points in time, as calculated using BST, in order to describe the evolution of the wave-spectrum in the wavenumber domain. Unfortunately, this gives no indication as to the dispersive properties of the wave group.

This limitation can be overcome by applying the ST. This is similar to a Wavelet transform, but has a direct relationship with the Fourier transform (Stockwell *et al.* 1996). It essentially performs the Fourier transform on a Gaussian windowed segment of a time trace, with the width of the window varying in frequency,

$$\mathrm{ST}(\tau, f) = \int_{-\infty}^{\infty} x(t) \frac{f}{\sqrt{2\pi}} \mathrm{e}^{-((\tau-t)^2 f^2/2)} \mathrm{e}^{(-\mathrm{i}2\pi f t)} \, \mathrm{d}t. \tag{4.2}$$

The ST gives amplitude as a function of both frequency and time and so, for time-scales larger than the window width, overcomes the problems associated with non-stationary data. The one-dimensional transform has been described above, but this can easily be extended to more dimensions (Mansinha *et al.* 1997). The two-dimensional ST has been applied to the results of BST in time and space. This allows changes to both the frequency and the wavenumber of the wave-components to be determined in both space and time. Therefore, both the evolution of the amplitude spectrum and changes to the dispersive properties of the wave group can be identified.

The focus of this paper is the evolution of the underlying linear spectrum. However, both the Fourier and the STs assume that the wave profile is the linear sum of various wave components. Hence, any *bound* nonlinearities are modelled by the inclusion of additional harmonics that represent wave components that are not freely propagating (*bound* waves). While this has parallels with wave theories based upon perturbation methods, it often means that it is difficult to identify which components are freely propagating. This can, to some extent, be overcome by separating a wave spectrum into its odd- and even-order wave components, as described in Johannessen & Swan (2003). If η_{p} defines the positive wave profile, corresponding to the focusing of wave crests and η_{n} the negative wave profile, corresponding to the focusing of wave troughs, it follows that

$$\begin{aligned}\eta(\boldsymbol{x})_{\mathrm{p}} = & \sum_i h_1(a_i, \boldsymbol{k}_i, d) + \sum_i \sum_j h_2(a_i a_j, \boldsymbol{k}_i, \boldsymbol{k}_j, d) \\ & + \sum_i \sum_j \sum_k h_3(a_i a_j a_k, \boldsymbol{k}_i, \boldsymbol{k}_j, \boldsymbol{k}_k, d) \\ & + \sum_i \sum_j \sum_k \sum_m h_4(a_i a_j a_k a_m, \boldsymbol{k}_i, \boldsymbol{k}_j, \boldsymbol{k}_k, \boldsymbol{k}_m, d) + \cdots,\end{aligned} \tag{4.3}$$

$$\begin{aligned}\eta(\boldsymbol{x})_{\mathrm{n}} = & -\sum_i h_1(a_i, \boldsymbol{k}_i, d) + \sum_i \sum_j h_2(a_i a_j, \boldsymbol{k}_i, \boldsymbol{k}_j, d) \\ & - \sum_i \sum_j \sum_k h_3(a_i a_j a_k, \boldsymbol{k}_i, \boldsymbol{k}_j, \boldsymbol{k}_k, d) \\ & + \sum_i \sum_j \sum_k \sum_m h_4(a_i a_j a_k a_m, \boldsymbol{k}_i, \boldsymbol{k}_j, \boldsymbol{k}_k, \boldsymbol{k}_m, d) - \cdots,\end{aligned} \tag{4.4}$$

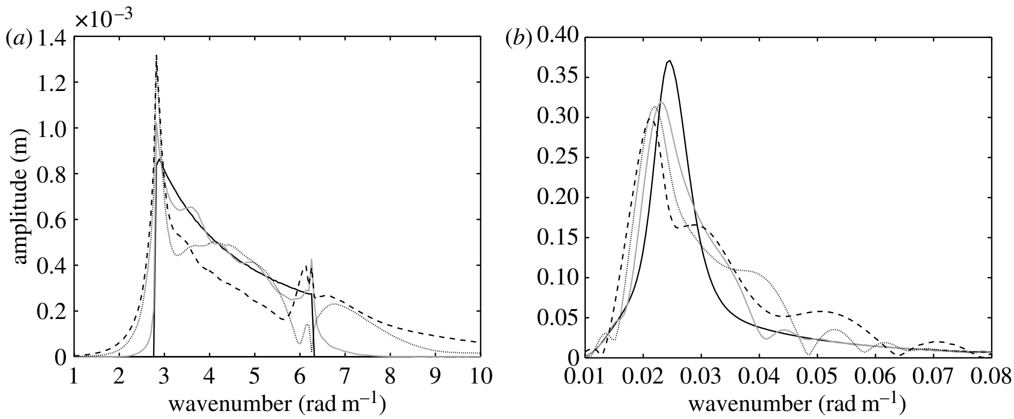

Figure 3. The evolution of odd-order spectra for (*a*) case NB and (*b*) case J5D0. Solid line: initial (*a*) $t=-200$ s, (*b*) $t=-1000$ s; grey line: (*a*) $t=-100$ s, (*b*) $t=-500$ s; dotted line: (*a*) $t=-20$ s, (*b*) $t=-300$ s; dashed line, extreme event: (*a*) $t=-9$ s, (*b*) $t=-166$ s.

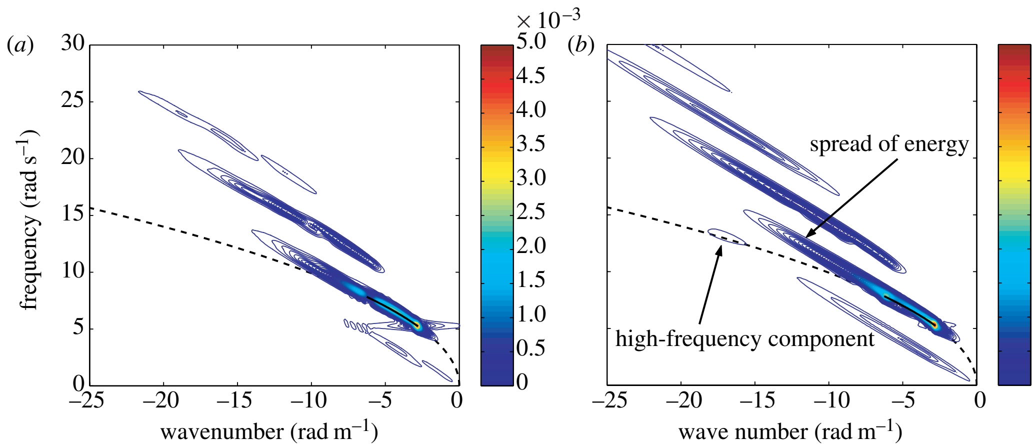

Figure 4. Amplitude of wave-components for case NB. (*a*) $t=-18.5$ s, $x=-18.2$ m and (*b*) $t=-9$ s, $x=-8.2$ m (extreme event). Dashed curve, linear dispersion; solid curve, input range.

where h are functions of the amplitudes a_i, wavenumber vectors $\mathbf{k}_i$ and water depth d, and hence, represent the various interactions. Comparisons between these results confirm that only the odd-order terms change sign. As a result, subtracting η_{n} from η_{p} defines the wave profile of the odd-order interactions,

$$\eta(\boldsymbol{x})_{\mathrm{odd}} = \frac{\eta_{\mathrm{p}} - \eta_{\mathrm{n}}}{2} = \sum_i h_1(a_i, \boldsymbol{k}_i, d) + \sum_i \sum_j \sum_k h_3(a_i a_j a_k, \boldsymbol{k}_i, \boldsymbol{k}_j, \boldsymbol{k}_k, d) + \text{odd terms.} \tag{4.5}$$

The wave profile of the odd-order interactions, η_{odd}, defines the profile of the freely propagating wave components provided two conditions are met: the third- and higher-order *bound* interactions are insignificant, which has been shown to be the case in §3; and the third-order *resonant* interactions dominate the evolution of the spectrum. The earlier laboratory results of Baldock *et al.* (1996) and Johannessen & Swan (2003) (discussed in §2) suggest that both of these conditions are indeed met. In the former, it was found that both extreme wave-crest events and extreme wave-trough events focused at the same point in the wave tank; if the fourth-order resonant interactions were significant then this would not be the case. In the latter, it was found that if the correct freely propagating wave components were identified, there was excellent agreement between the surface profile and the underlying water-particle kinematics predicted by the second-order solution of Sharma & Dean (1981) and those predicted by the fully nonlinear model of Johannessen & Swan (2003). If the third-order *bound* interactions were significant, this would not be the case. Hence, the spectrum of the odd-order profile is a very good approximation of the spectrum of the freely propagating wave components (the free-wave spectrum). In addition, it is also possible to isolate the profile of the even-order components by adding the positive wave profile to that of the negative, $\eta_{\text{even}}=(\eta_{\text{p}}+\eta_{\text{n}})/2$. The spectrum of this profile predominantly contains the results of the second- and higher-order *bound* wave interactions, but also contains any fourth- and higher-order *resonant* interactions.

(i) *Unidirectional sea-states*

Figure 3 depicts the evolution of the odd-order spectrum during the formation of an extreme wave event in the unidirectional sea-states of cases NB and J5D0. It is apparent that in both these examples, there are significant changes to the amplitude of the freely propagating wave components. These manifest themselves as a widening of the free-wave regime. What is also apparent is the speed at which the spectra evolve; there are significant changes to both spectra in the 10 wave periods before the extreme event. The speed of these interactions is in direct contrast to the slow evolution predicted in random sea-states by Hasselmann (1962). Although, these sea-states are anything but random, they are representative of how large waves evolve. While both of these spectra are fairly narrow-banded, significant changes are also observed in all of the unidirectional cases in table 1. However, it should be noted that narrow-banded sea-states, such as J5D0, are typically more nonlinear than those that are more broad-banded, such as J1D0. As a result, it is clear that the 'peakedness' of unidirectional spectra is an important factor in determining their evolution.

The ST has also been applied to these two unidirectional cases in order to ascertain the changes to the wave spectra in wavenumber and wave frequency between different points in time and space. This is shown in figures 4 and 5, where the time and location (t, x) at which the transform has been applied is indicated in the figure captions. In these figures, the wavenumber is considered to be negative and hence consistent with the definition of the surface elevation, $\eta(\boldsymbol{x})=\sum_i a_i \sin(\omega t-\boldsymbol{kx})$. In a separate study, the transform has been successfully applied in order to identify wave components travelling in different directions. In both figures 4 and 5, there are a number of clearly identifiable 'ridges' representing (in order from top to bottom), the third-order sum components (*bound*), the second-order sum components (*bound*), the linear components (*free*) and the second-order difference components (*bound*).

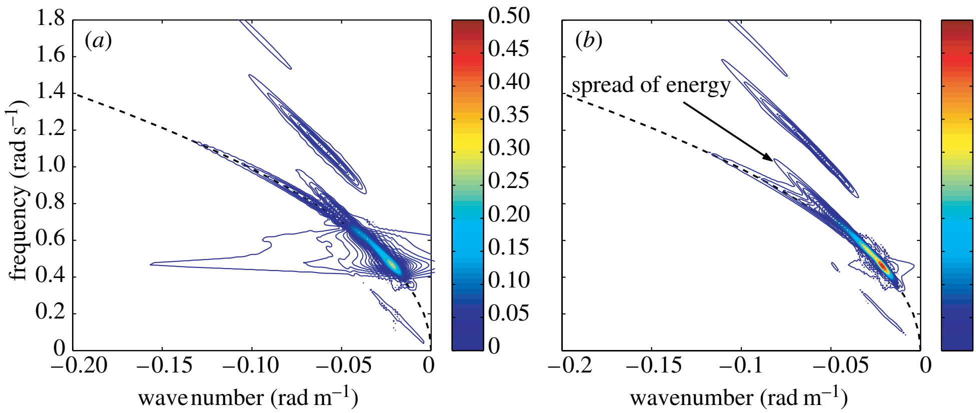

Figure 5. Amplitude of wave-components for case J5D0. (*a*) At $t = -294$ s, $x = -2500$ m and (*b*) at the time and location of the extreme event, $t = -166$ s, $x = -1416$ m. Dashed curve, linear dispersion; solid curve, input range.

These figures show that in both cases, the amplitude of the *bound* components increases as the wave group evolves towards the extreme event. This is not surprising and merely represents the fact that the profile is steeper around the extreme crest. This can be interpreted in terms of a perturbation analysis as the need for higher harmonic terms to satisfy the nonlinear boundary conditions. However, the figure also shows changes to the linear components. In particular, there is a growth of a spread of energy that almost, but not quite, satisfies the linear dispersion relationship (indicated by the dashed line). This spread of energy forms a distinct group in case NB, but merges with the linear components in case J5D0. The origins of this spread of wave energy are not clear. Indeed, three suggestions seem plausible: (i) third-order difference energy of the form $\omega_0 + \omega_1 - \omega_2$, (ii) freely propagating components that are travelling faster than would be predicted by linear theory, and (iii) harmonics that are included to represent the non-stationarity of the data, and hence, this is not 'real' wave energy. The physical mechanisms responsible for this spread of energy and the reasons why it does not satisfy the linear dispersion relationship are investigated in §5 through the use of ZE. However, the spread of wave energy can also be investigated by applying the ST to the profiles of both the odd- and even-order components. Figure 6*a* shows a close up of the former for case NB at the time and location of the extreme event and indicates that the spread of energy is an odd-order interaction. Whereas, figure 6*b* shows the latter and highlights a high-frequency component that, although small in magnitude, is a clear example of an even-order resonant interaction.

(ii) *Directional sea-states*

The evolution of the directional wave spectra of cases J5D5 and J5D30 have been investigated by examining the differences between the odd-spectrum at the initial time, as shown in figures 7*a* and 8*a*, with that at the time of the extreme wave event, figures 7*b* and 8*b*. These spectra only include the freely propagating

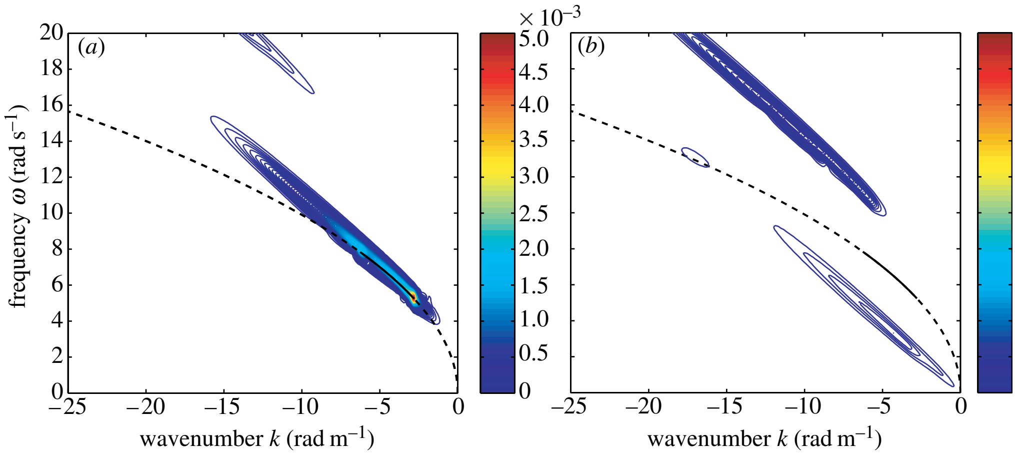

Figure 6. Amplitude of wave-components for case NB. (*a*) Odd-order components and (*b*) even-order components at the extreme event, $t = -9$ s, $x = -8.2$ m. Dashed curve, linear dispersion; solid curve, input range.

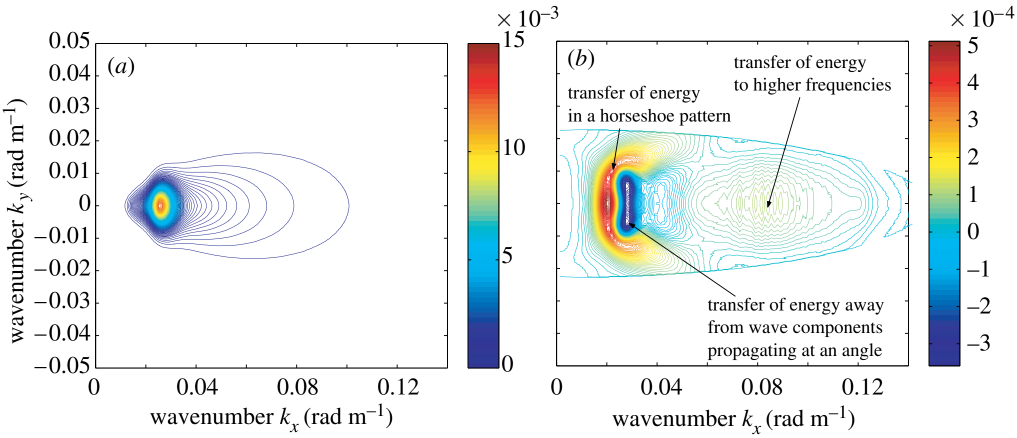

Figure 7. The evolution of the odd-spectrum of case J5D5. (*a*) Initial spectrum a_i^{initial} and (*b*) difference between the spectrum at the time of the extreme event and the initial spectrum, $a_i^{\text{diff}} = a_i^{\text{event}} - a_i^{\text{initial}}$. The contours define the amplitude, a_i, of the wave components.

wave components, and hence, this analysis shows the effect of the resonant evolution of the free-wave regime. The changes to the free-wave regime and their effect on the directional spread of the wave group will be discussed here. The importance of the degree of directional spreading on the consequences of the spectral evolution will be highlighted later.

The most important change that occurs is the reduction in energy propagating at an angle to the mean wave direction. This feature of the evolution can be identified in both short- and long-crested sea-states and the angle at which it occurs is similar to that of the spreading parameter of the input spectrum: 6° for case J5D5; and 31° for case J5D30. On its own, this would lead to a *reduction* in the directional spread of the wave group. However, there is also a further feature of the evolution that is important in long-crested sea-states: the transfer of energy into a horseshoe pattern around the peak. This leads to an *increase* in the directional spread of the wave group. The evolution of directional wave groups also has two features that are similar to those found in unidirectional wave groups; first, there is a spread of energy to higher wavenumbers and secondly, a transfer of energy away from the peak of the spectrum.

In contrast to unidirectional sea-states, figure 9*a*,*b* show that in defining the resonant evolution, the peakedness of the spectrum is less important than the directional spreading. Evidence of this is provided by the fact that the various features of the energy transfers are very similar for the pair J5D5 and J1D5 (figure 9*a*), and also for the pair J5D30 and J1D30 (figure 9*b*). However, there is a marked contrast between J5D5 and J5D30, and between J1D5 and J1D30. Therefore, the conclusion (so far) would be that the evolution of directional spectra depends upon the spreading parameter, σ_{s}, rather than the peakedness, γ. However, this is slightly misleading as the extreme wave event occurs much earlier in the long-crested case J5D5 than it does in the short-crested case J5D30. Hence, the phasing of the wave components in the two cases is very different. If the initial phasing of the wave components in the two cases is determined iteratively, such that a perfectly focused wave event occurs (one in which all of the components come exactly into phase at one point in space and time), the maximum crest elevation remains largely unchanged, but the evolution of the two spectra is now remarkably similar. This is shown in figure 10 and highlights the importance of the phasing of the wave components in determining the evolution of the wave spectra. The changes in the degree of directional spreading of these sea-states is shown in figure 11 in terms of the mean angle $\theta_{\mathrm{m}} = [\sum_N a_i |\theta_i|]/A$, where A is the amplitude sum of the underlying linear wave components defined by $A = \sum_i^N a_i$ and θ_i the angle of propagation of a wave component i. This not only confirms that the phasing of the wave components is fundamental to the evolution of these spectra, but also highlights the fact that, while the evolution is rapid, it is more gradual than that observed in unidirectional sea-states.

5. Physical mechanisms

In §4, it was shown that during the formation of an extreme wave event, the wave spectrum could change both significantly and rapidly. In §3, it was shown that these changes could lead to an extreme event that is much higher and steeper than a *bound* wave solution would predict. It is the purpose of this section to explain the physical mechanisms that cause these changes. Using these results, the significant differences in the evolution of unidirectional and directional sea-states will be ascertained. Literature concerning the transfer of energy between wave components is discussed in detail in the review articles of Yuen & Lake (1980), Hammack & Henderson (1993) and, in the context of wave breaking, Banner & Peregrine (1993). Although much of this work is relevant, only those interactions that are significant to the present discussion are highlighted below. Accordingly, as significant changes to the height and shape of the largest waves must necessarily involve the interaction of wave components having appreciable energy, interactions involving the shortest wave components, in the extreme tail of the spectrum are neglected. These wave components may provoke highly localized wave instabilities that mark the onset of wave breaking, but are unlikely to play a dominant role in defining the shape of an extreme wave event.

In §1, it was noted that deep-water *resonant* interactions must involve the interaction of three or more wave components ($N \geq 3$ in equations (1.1a) and (1.1b)), and hence, can only occur at third order and above. In terms of ZE, the $\tilde{V}$ kernel governs the third-order ($N=3$) resonance and the $\tilde{W}$ kernel the fourth-order ($N=4$) resonance (equation (3.7)). While it is clear that if energy is transferred between wave components their amplitudes must alter, if energy is transferred to a wave component 'out of phase' with energy that is already there, the dispersive properties of that component will also change. This was shown for pairs of wave components by Longuet-Higgins & Phillips (1962), and is the mechanism by which the Benjamin & Feir (1967) instability allows for the *near-resonant* interactions between unidirectional wave components. When such interactions involve only one ($k_0 = k_1 = k_2 = k_3$) or two wave components ($k_0 = k_1$ and $k_2 = k_3$), there is a change in their phase speed, but no change in their amplitude. In the first case, this corresponds to the Stokes (1847) third-order correction to the phase speed; while in both cases such interactions are often termed *degenerate*. However, when more components are involved, the *resonant* interactions are capable of altering both their amplitude and their dispersive properties.

By applying ZE with only the $\tilde{V}$ kernel in equation (3.7), it is possible to ascertain the effect of third-order *resonant* interactions on the evolution of the spectrum. This has been undertaken for the unidirectional and directional spectra considered previously.

(a) *Unidirectional sea-states*

Figures 13 and 14 show a comparison between the results of ZE, based on the inclusion of only the third-order *resonant* terms ($\tilde{V}$), with those of the odd-spectrum of BST for cases NB and J5D0, respectively. In order to make this comparison, the amplitude spectra associated with ZE and BST have been normalized with respect to the largest input amplitude at $t = t_0$. This is undertaken to overcome differences in discretization between the two models. Therefore, figures 13 and 14 show the changes in the amplitudes of the wave components between $t = t_0$ and the time at which the wave focuses. An important issue is the effect of discretization on the results of the wave models; for BST this is addressed in Bateman & Swan (submitted), whereas for ZE this is addressed in figure 12, which shows that for case NB the solution is converging rapidly.

It is clear from figures 13 and 14 that ZE can model the rapid evolution of the wave spectrum, with excellent agreement between the two wave models. As a result, it can be concluded that the spread of energy to high wavenumbers is predominantly the result of third-order *resonant* interactions. Furthermore, by including the $\tilde{W}$ function in equation (3.7), it is possible to show that the higher-order *resonant* interactions are insignificant to the evolution of these spectra.

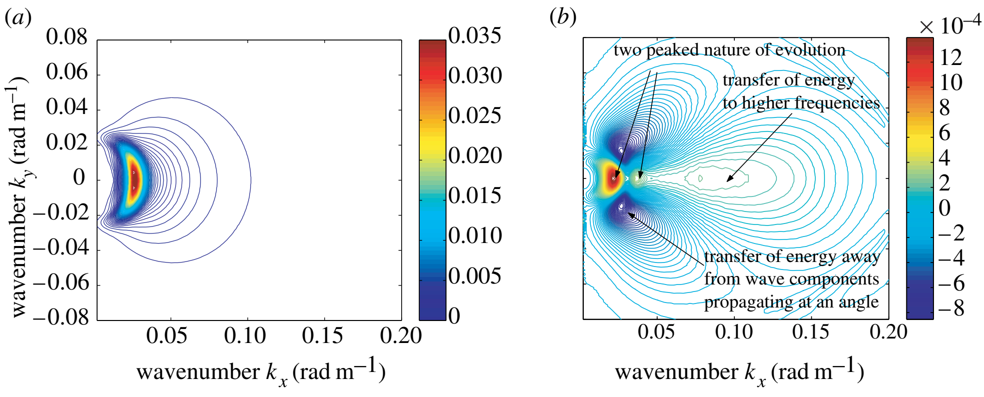

Figure 8. The evolution of the odd-spectrum of case J5D30: (*a*) initial spectrum a_i^{initial}; (*b*) difference between the spectrum at the time of the extreme event and the initial spectrum: $a_i^{\text{diff}} = a_i^{\text{event}} - a_i^{\text{initial}}$. The contours define the amplitude, a_i, of the wave components.

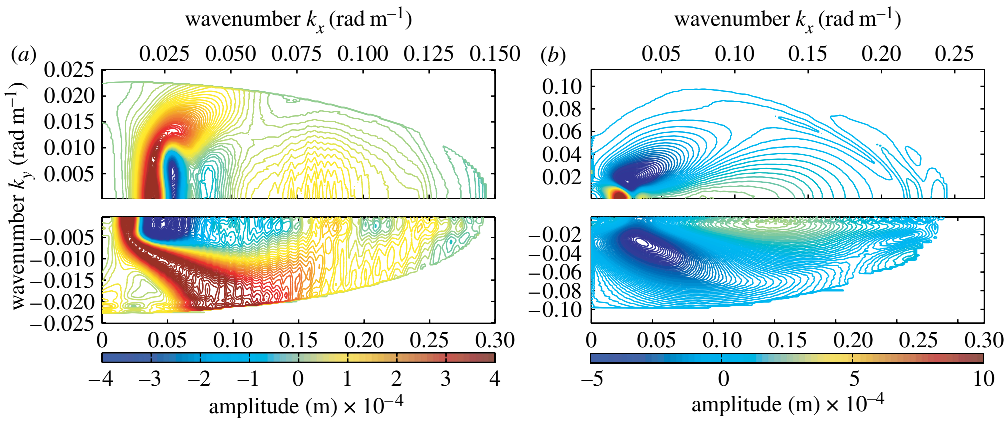

Figure 9. Comparison between the evolution of spectra with different peak-enhancement factors. (*a*) J5D5 upper, J1D5 lower and (*b*) J5D30 upper, J1D30 lower. The contours represent the difference between the spectrum at the time of the extreme event and the initial spectrum, $a_i^{\text{diff}} = a_i^{\text{event}} - a_i^{\text{initial}}$.

This is shown for case NB in figure 15. In this case, the greatest difference between the third- and fourth-order results is in the region $k > 15$ rad m^{-1}, which lies outside our main area of interest. However, it does correspond to where the small high-frequency component ($k = 16$ rad m^{-1}, $\omega = 1.25$ rad s^{-1}) was observed in figure 6*b*, suggesting that the latter is the result of a fourth-order *resonant* interaction. These results are in agreement with work on unidirectional random wave trains undertaken by both Mori & Yasuda (2002) and Janssen (2003). The former found that the largest waves only occur if interactions higher than those of second-order are included. Whereas, the latter stressed the importance of the Benjamin–Feir instability to the formation of large waves, and its role in the widening of the wave spectrum.

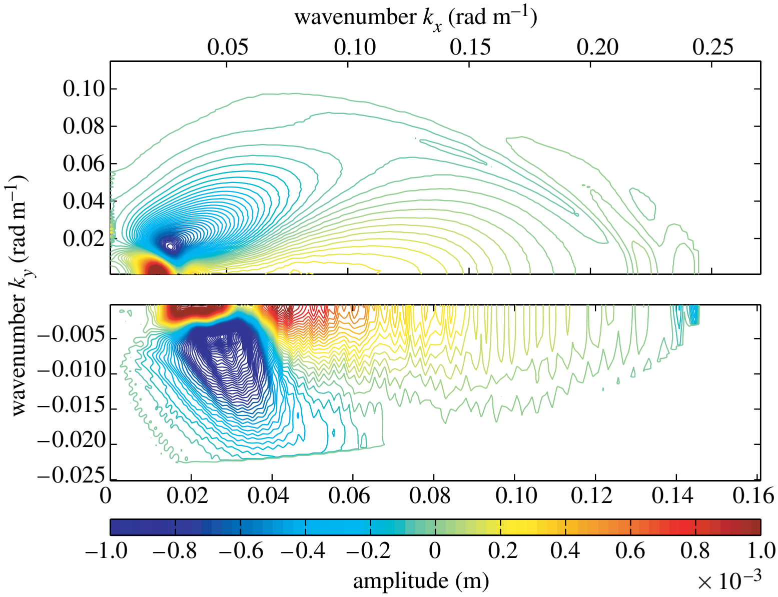

Figure 10. Comparison between the evolution of spectra with different spreading in sea-states in which a perfectly focused wave event occurs. J5D30 upper, J5D5 lower. The contours represent the difference between the initial spectrum and the spectrum at the time of the extreme event, $a_i^{\mathrm{diff}} = a_i^{\mathrm{event}} - a_i^{\mathrm{initial}}$.

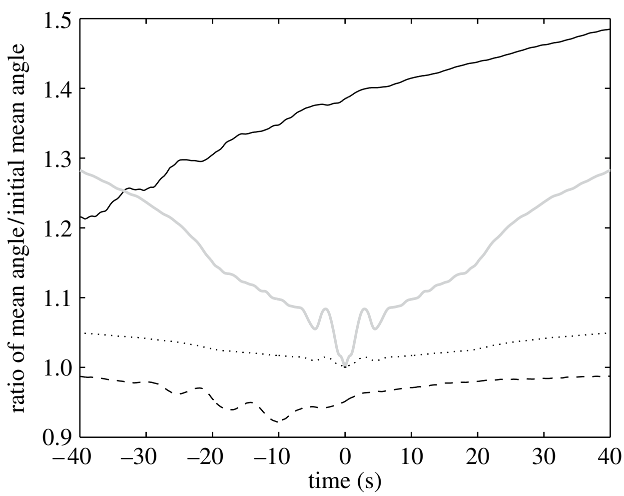

Figure 11. Changes to the mean angle of cases J5D5 and J5D30 during the formation of an extreme wave event. Solid line, J5D5 initial phasing derived from linear theory; grey line, J5D5 initial phasing determined to form a perfectly focused event; dashed line, J5D30 phasing derived from linear theory; dotted line, J5D30 initial phasing determined to form a perfectly focused event.

Figures 4 and 5 in §4 showed that in all cases, the spread of energy to high wavenumbers did not exactly satisfy the linear dispersion relationship. However, figures 13 and 14 show that the spread of energy is the result of third-order *resonant* interactions, and hence, the wave components are freely propagating.

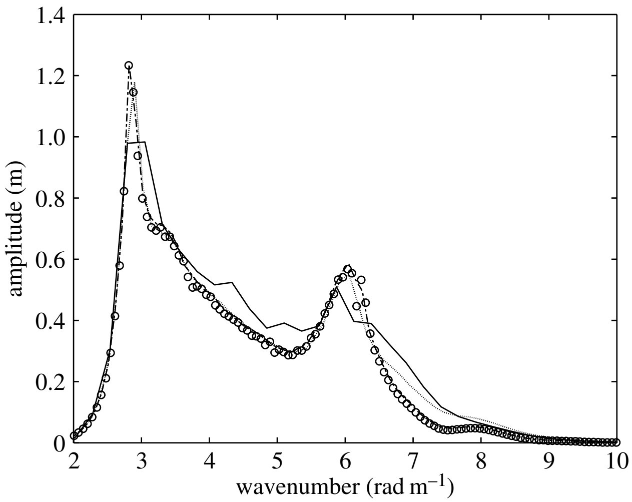

Figure 12. The effect of the number of wave components on the evolution of case NB. Solid line, 40; dotted line, 60; dash-dotted line, 100; open circle, 150.

The reason for this apparent discrepancy can be investigated by applying ZE in order to ascertain, for a given wavenumber, the frequency of each wave component. Furthermore, ZE can be used to isolate the effect of different physical processes on this frequency. Three effects are of particular significance: (i) the frequency from the linear dispersion relationship in deep water can be calculated as $\omega_1=\sqrt{gk}$, (ii) the change in the frequency due to *degenerate* third-order *resonant* interactions that occur when a wave component interacts with itself (the Stokes change to the phase velocity) and when two wave components interact with one another (Longuet-Higgins 1962), can be calculated as ω_3, and (iii) the instantaneous frequency ω_i can be calculated as the rate of change of the phase of each component (Cohen 1995). Figure 16 shows the instantaneous frequency for case NB both at the focal event ($t=-9$ s) and at a time well before the focal event ($t=-199$ s). At $t=-199$ s, the difference between the instantaneous frequency and the linear dispersion relationship is small. Furthermore, for components of significant amplitude, which lie in the range $2.5<k<6.0$ rad m^{-1}, the degenerate resonant interactions explain the difference. However, it is clear that at $t=-9$ s, the wave-components no longer satisfy the linear dispersion relationship. Furthermore, at $t=-9$ s, the degenerate *resonant* interactions make an insignificant contribution to the instantaneous frequency.

Figure 17 shows the results from the application of ZE, at $t=-9$ s, superimposed upon those of the ST (figure 4*b*). There is excellent agreement between the wavenumbers and instantaneous frequencies calculated by ZE, indicated by the red line, and those from the application of the ST. Furthermore, as ZE has been applied using only the third-order *resonant* terms, the physical processes responsible for the change in the phase velocity of the wave components are immediately obvious; energy is being transferred to existing wave-components 'out of phase' with the energy that is already present and, as a result, the dispersive properties of the wave group have been altered.

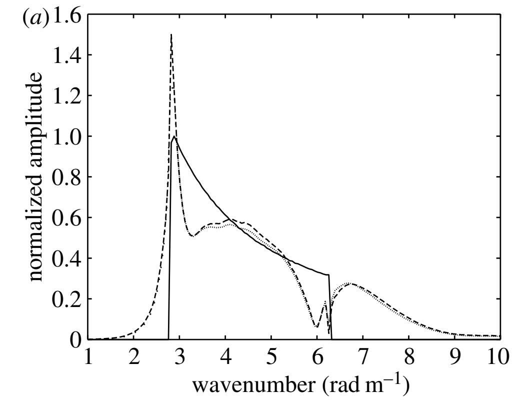

Figure 13. Evolution of the free-wave spectrum of case NB. Comparisons are shown between BST and ZE, where the latter only includes the third-order resonant terms. (*a*) $t=-20$ s, (*b*) $t=0$ s. Solid line, initial; dashed line, BST; dotted line, ZE.

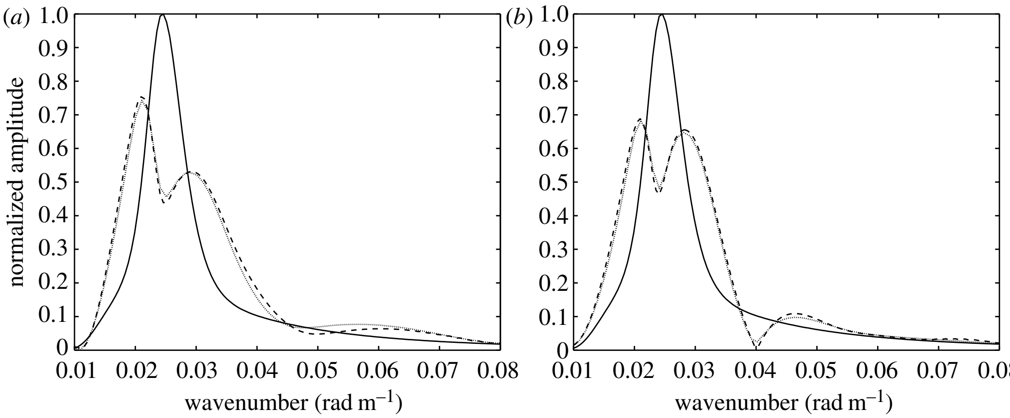

Figure 14. Evolution of the free-wave spectrum of case J5D0. (*a*) $t=-100$ s, (*b*) $t=0$ s. Solid line, initial; dashed line, BST; dotted line, ZE.

Therefore, it is proven that the spread of energy identified in §4 is the result of freely propagating wave components travelling faster than might be expected by linear theory.

(*b*) *Directional sea-states*

The results of ZE, applied with only the third-order *resonant* terms included, have been compared to those of BST for the directional spread cases J5D5 and J5D30. In contrast to the unidirectional cases, these comparisons are difficult because, owing to computational limitations, the number of components over which the spectra are discretized is very different for the two models; BST uses 16 384 wave components, whereas ZE only 400. However, it is possible to compare the properties of the wave spectra, particularly the amplitude sum, A, and the mean angle, θ_{m}. Figure 18 confirms that the main features of the

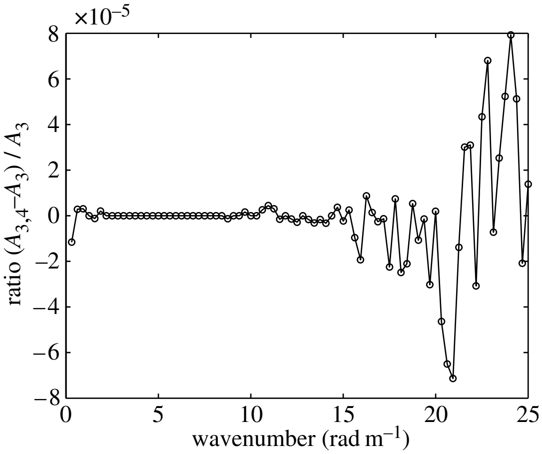

Figure 15. Difference between the evolution of the free-wave spectrum of case NB at $t=0$ s. The vertical axis represents the difference in the amplitude of the wave components calculated using both the third- and fourth-order resonant terms, $A_{3,4}$, over that calculated using only the third-order terms, A_3.

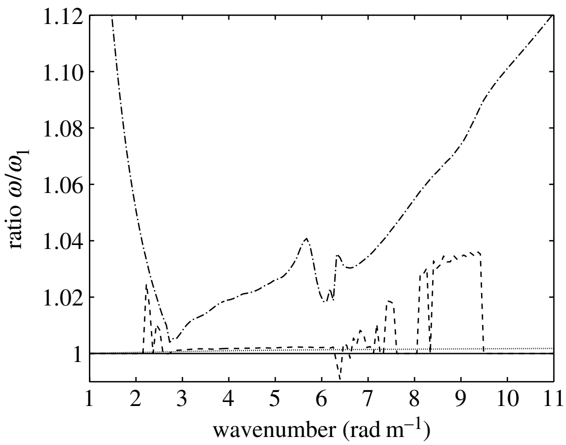

Figure 16. Changes to the dispersive properties of the wave group of case NB. Solid line, linear ω_1; dotted line, self-interaction ω_3 at all times; dashed line, instantaneous frequency ω_i at $t=-199$ s; dash-dotted line, instantaneous frequency ω_i at $t=-9$ s.

evolution of the wave groups can be identified using either model. In long-crested sea-states, there is a gradual, but significant, increase in both the amplitude sum and the mean angle, whereas in short-crested sea-states both slightly reduce around the extreme event. However, as discussed earlier, these results are strongly influenced by the phasing of the wave components. For example, if this is adjusted iteratively to ensure that the wave group focuses perfectly, figure 19 shows that in the long-crested sea (case J5D5) far from increasing, the amplitude sum actually reduces, an effect reproduced by both models.

The results presented in figures 18 and 19 indicate that the evolution of the wave spectra is primarily the result of third-order *resonant* interactions. Therefore, the evolution of both unidirectional and directional spectra is

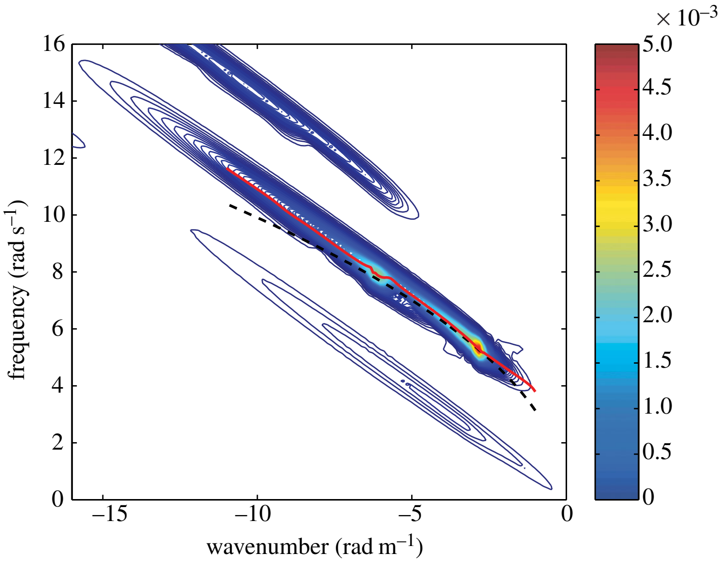

Figure 17. Comparison between the dispersive properties of the wave group of case NB calculated using ZE with that indicated by the application of the ST at $t=-9$ s. The contours represent the amplitude of the wave components, the linear dispersion relationship (dashed curve) and the dispersion relationship calculated using ZE (solid curve).

controlled primarily by the same physical mechanisms. However, the consequences of these changes are very different. Indeed, the evidence presented so far indicates that the extreme crest-elevation associated with a focused wave event in a unidirectional sea cannot be predicted by a *bound*-wave solution. In contrast, in a directional sea the extreme crest elevation is reasonably well predicted by a *bound*-wave solution, but the overall shape of the wave profile is not, particularly, the wave steepness and the depth of the adjacent troughs.

6. Conclusions

It has been shown that the formation of large ocean waves cannot be explained in terms of a constant spectrum of freely propagating wave components coupled with their associated *bound* waves. In both unidirectional and directionally spread seas, the evolution of a large wave event involves rapid changes to the spectrum of the freely propagating wave components. In both cases, this evolution is primarily the result of third-order *resonant* interactions that are capable of altering not only the amplitude of wave components, but also their relative phasing. However, the consequences of these changes can be very different; in unidirectional sea-states the extreme crest is higher than second-order theory would predict, whereas, in directionally spread sea-states, it is typically lower. With all the events close to their breaking limit, these changes cannot simply be explained in terms of differences in the inline wave-front steepness. Similarly, reductions in the time available for the interactions to occur as the directionality increases does not fully explain these differences. Indeed, the present results have shown that there are fundamental differences in the

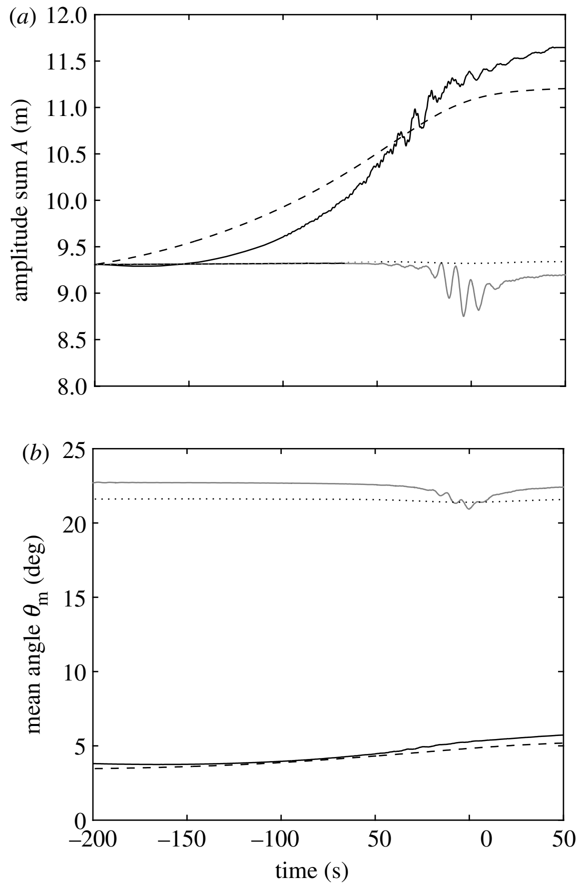

Figure 18. Changes to the properties of the free-wave spectra of cases J5D5 and J5D30 as calculated using ZE and BST. (*a*) The amplitude sum, A, (*b*) the mean angle, θ_{m}. Solid line, J5D5 BST; dashed line, J5D5 ZE; grey line, J5D30 BST; dotted line, J5D30 ZE.

evolution of the largest waves depending on the directionality of the wave-field; the explanation for which lies in the nonlinear changes to the spectral bandwidth and the phasing of the wave components.

In unidirectional seas, the spectral evolution involves a rapid and significant broadening, with energy transferred to high frequencies; whereas, in directional seas the degree of directional spreading can change, but the manner in which it changes critically depends upon the phasing of the wave components. These two features are related; changes to the directional spread of a spectrum are closely linked to changes in the bandwidth. Moreover, changes to the bandwidth of a spectrum alter its amplitude sum, $A=\sum_i^N a_i$, allowing the possibility of larger maximum crest elevations. This occurs because the total energy, which must remain constant, is proportional to the sum of the squares of the amplitude of the wave components, $E=\sum_i^N a_i^2$. If the amplitude sum, A, is spread evenly over N wave components, $a_i=A/N$, it follows that $A=\sqrt{N}\sqrt{E}$. The amplitude sum of the spectrum is thus proportional to the square root of the number of

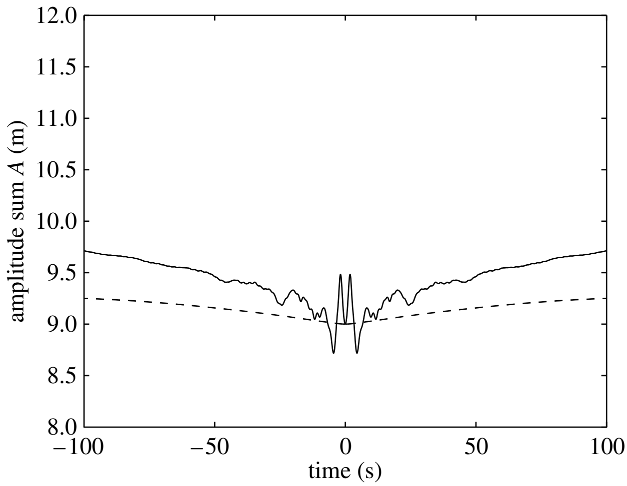

Figure 19. Changes to the amplitude sum of the free-wave spectra of case J5D5, where in contrast to figure 18*a* the wave event is perfectly focused. Solid line, J5D5 BST; dashed line, J5D5 ZE.

components over which the amplitude is spread. Therefore, it follows that as a spectrum becomes more broad banded (N increases), its amplitude sum increases.

The broadening of unidirectional spectra (figure 3) is therefore consistent with an increase in their amplitude sum, and hence, larger maximum crest elevations. In contrast, in directional seas, the results emphasize the balance between changes to the focal quality (the degree to which the wave components come into phase) and changes to the amplitude sum; as the focal quality increases the amplitude sum reduces. This suggests that the largest wave in a directional sea-state may not be perfectly focused. However, after exhaustive investigation into the most probable shape of the highest crest elevations arising in a sea described by a JONSWAP spectrum, the focal quality was found to be the dominant factor. Hence, in JONSWAP sea-states, the most probable highest wave is one that is almost perfectly focused. This is consistent with the analysis of field data described by Jonathan *et al.* (1994).

These arguments suggest that it is not possible to obtain large nonlinear increases in crest elevation in broad-banded directionally spread seas. Alternatively, acknowledging the balance between the effects of dispersion or focal quality, and changes in the amplitude sum of the spectrum, implies that large nonlinear increases in crest elevation may occur in directional seas that are initially narrow-banded and are therefore slow to disperse. This raises an important question: are sea-states dominated by swell waves more likely to exhibit large nonlinear increases in crest elevation?

To begin to answer this question, the evolution of a large wave event in a Gaussian spectrum has been considered. This example corresponds to case G16D5 in table 1; it has a small directional spread, $\sigma_s = 5°$, and is representative of a sea-state that is swell dominated. Figure 20*a* confirms that the formation of an extreme wave event leads to a significant broadening of the spectrum; while, figure 20*b* indicates that, as expected, this broadening leads to a significant increase in the amplitude sum A. More importantly, figure 20*c* confirms that the

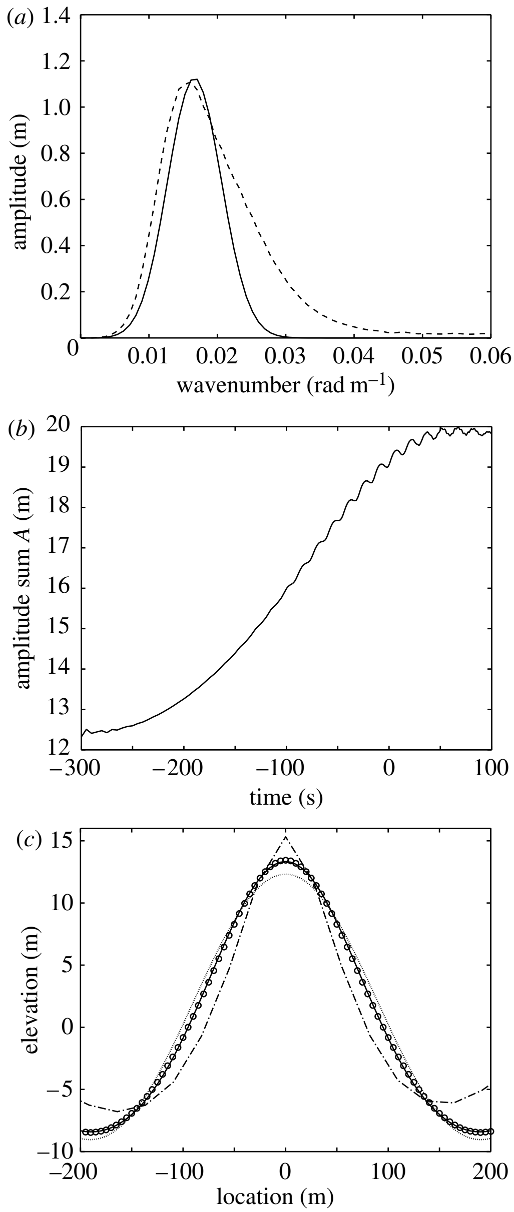

Figure 20. The evolution of a swell-dominated sea, case G16D5. (*a*) Changes in the amplitude spectrum of freely propagating wave components summed over all angles. Solid line, initial spectrum; dashed line, spectrum at the time of the largest event. (*b*) The amplitude sum, A, of the freely propagating wave components. (*c*) The extreme wave profile: comparisons between the fully nonlinear calculations of BST and linear, second- and third-order solutions. Dotted line, linear; solid line, second-order; open circle, third-order; dash-dotted line, fully nonlinear.

extreme wave profile is both steeper and higher than would be predicted by a *bound* wave solution. This result suggests that the rapid and local spectral evolution necessary to explain unexpectedly large crest elevations, and hence, *freak* or *rogue* waves, may be intrinsically more likely to occur in severe swell-dominated seas rather than in locally generated wind seas. However, given that such sea-states are rare, several equally important questions arise. For example, how narrow-banded, in both frequency and direction, must a spectrum be in order for the *resonant* nonlinearities to dominate over the effects of dispersion? Furthermore, what effect does the presence of wind waves have on the evolution of a swell-dominated sea? Having identified the mechanics responsible for the evolution of a free-wave spectrum, these important questions are the subject of on-going research.

The early stages of this work were undertaken within the project 'Reliability Based Structural Design of FPSO Systems', which involves Shell, Instituto Superior Técnico, DHI, Det Norske Veritas, Imperial College, Noble Denton and Oxford University. The project is partially funded by the European Union through the Energy Programme under contract ENK6-2000-00107. The later stages of the work were completed with support from the UK Engineering and Physical Sciences Research Council under grant number GR/R64971.

References

Airy, G. B. 1845 Tides and waves. In *Encyclopaedia metropolitana*, vol. 5, pp. 241–396. London.

Annenkov, S. & Shrira, V. 2001 Numerical modelling of water-wave evolution based upon the Zakharov equation. *J. Fluid Mech.* **449**, 341–371.

Baldock, T. E., Swan, C. & Taylor, P. H. 1996 A laboratory study of nonlinear surface waves on water. *Phil. Trans. R. Soc. A* **354**, 649–676.

Banner, M. & Peregrine, D. 1993 Wave breaking in deep water. *Annu. Rev. Fluid Mech.* **25**, 373–397. (doi:10.1146/annurev.fl.25.010193.002105)

Bateman, W. J. D. & Swan, C. Submitted. Realistic descriptions of extreme ocean waves. Part 1: the application of recent advances in wave modelling.

Bateman, W. J. D., Swan, C. & Taylor, P. H. 2001 On the efficient numerical simulation of directionally-spread surface water waves. *J. Comput. Phys.* **174**, 277–305. (doi:10.1006/jcph.2001.6906)

Benjamin, T. B. & Feir, J. E. 1967 The disintegration of wavetrains on deep water. *J. Fluid Mech.* **27**, 417–430. (doi:10.1017/S002211206700045X)

Boccotti, P. 1983 Some new results on statistical properties of wind waves. *Appl. Ocean Res.* **5**, 134–140. (doi:10.1016/0141-1187(83)90067-6)

Cohen, L. 1995 *Time-frequency analysis*. Englewood Cliffs, NJ: Prentice-Hall.

Craig, W. & Sulem, C. 1993 Numerical simulation of gravity waves. *J. Comput. Phys.* **108**, 73–83. (doi:10.1006/jcph.1993.1164)

Fenton, J. D. & Rienecker, M. M. 1982 A Fourier method for solving nonlinear water-wave problems: application to solitary-wave interactions. *J. Fluid Mech.* **118**, 411–443. (doi:10.1017/S0022112082001141)

Frigo, M. & Johnson, S. G. 1998 FFTW: an adaptive software architecture for the FFT. In *Proc. ICASSP Conf., Seattle, WA, USA*, vol. 3, pp. 1381–1384.

Hammack, J. & Henderson, D. 1993 Resonant interactions among surface water waves. *Annu. Rev. Fluid Mech.* **25**, 55–97. (doi:10.1146/annurev.fl.25.010193.000415)

Hasselmann, K. 1962 On the nonlinear energy transfer in a gravity wave system. Part 1. *J. Fluid Mech.* **12**, 481–500. (doi:10.1017/S0022112062000373)

Janssen, P. 2003 Nonlinear four-wave interactions and freak waves. *J. Phys. Oceanogr.* **33**, 863–884. (doi:10.1175/1520-0485(2003)33<863:NFIAFW>2.0.CO;2)

Johannessen, T. B. & Swan, C. 2001 A laboratory study of the focusing of transient and directionally spread surface water waves. *Proc. R. Soc. A* **457**, 971–1006. (doi:10.1098/rspa.2000.0702)

Johannessen, T. B. & Swan, C. 2003 On the nonlinear dynamics of wave groups produced by the focusing of surface-water waves. *Proc. R. Soc. A* **459**, 1021–1052. (doi:10.1098/rspa.2002.1028)

Jonathan, P., Taylor, P. H. & Tromans, P. S. 1994 Storm waves in the northern North Sea. In *Proc. Conf. on the Behaviour of Offshore Structures, BOSS'94*, vol. 2, pp. 481–494. Boston, MA: MIT.

Krasitskii, V. P. 1994 On reduced equations in the Hamiltonian theory of weakly nonlinear surface waves. *J. Fluid Mech.* **272**, 1–20. (doi:10.1017/S0022112094004350)

Lindgren, G. 1970 Some properties of a normal process near a local maximum. *Ann. Math. Stat.* **41**, 1870–1883.

Longuet-Higgins, M. 1962 Resonant interactions between two trains of gravity waves. *J. Fluid Mech.* **12**, 321–332. (doi:10.1017/S0022112062000233)

Longuet-Higgins, M. & Phillips, O. 1962 Phase velocity effects in tertiary wave interactions. *J. Fluid Mech.* **12**, 333–336. (doi:10.1017/S0022112062000245)

Longuet-Higgins, M. S. & Stewart, R. W. 1960 Changes in the form of short gravity waves. *J. Fluid Mech.* **8**, 565–583. (doi:10.1017/S0022112060000803)

Mansinha, L., Stockwell, R. G., Lowe, R. P., Eramian, M. & Schincariol, R. A. 1997 Local S-spectrum analysis of 1-D and 2-D data. *Phys. Earth Planet. Inter.* **103**, 329–336. (doi:10.1016/S0031-9201(97)00047-2)

Milder, D. 1977 A note regarding 'On Hamilton's principle for surface waves'. *J. Fluid Mech.* **83**, 159–161. (doi:10.1017/S0022112077001116)

Mori, N. & Yasuda, T. 2002 Effects of high-order nonlinear interactions on unidirectional wave trains. *Ocean Eng.* **29**, 1233–1245. (doi:10.1016/S0029-8018(01)00074-9)

Phillips, O. M. 1960 On the dynamics of unsteady gravity waves of finite amplitude. *J. Fluid Mech.* **9**, 193–217. (doi:10.1017/S0022112060001043)

Rasmussen, J. H. & Stiassnie, M. 1999 Discretization of Zakharov's equation. *Eur. J. Mech. B/Fluids* **427**, 353–364. (doi:10.1016/S0997-7546(99)80033-8)

Sharma, J. N. & Dean, R. G. 1981 Second-order directional seas and associated wave forces. *Soc. Pet. Eng. J.* **4**, 129–140.

Shemer, L., Jiao, H., Kit, E. & Agnon, Y. 2001 Evolution of a nonlinear wave field along a tank: experiments and numerical simulations based upon the spatial Zakharov equation. *J. Fluid Mech.* **427**, 107–129. (doi:10.1017/S0022112000002305)

Stiassnie, M. & Shemer, L. 1984 On modifications of the Zakharov equation for surface gravity waves. *J. Fluid Mech.* **143**, 47–67. (doi:10.1017/S0022112084001257)

Stockwell, R. G., Mansinha, L. & Lowe, R. P. 1996 Localization of the complex spectrum: the S-transform. *IEEE Trans. Signal Process.* **44**, 998–1001. (doi:10.1109/78.492555)

Stokes, G. G. 1847 On the theory of oscillatory waves. *Trans. Camb. Phil. Soc.* **8**, 441–455.

Tromans, P. S., Anaturk, A. & Hagemeijer, P. 1991 A new model for the kinematics of large ocean waves—application as a design wave. In *Proc. 1st Offshore and Polar Engineering Conf. (ISOPE), Edinburgh*, vol. 3, pp. 64–71.

Yuen, H. & Lake, B. 1980 Instabilities of waves on deep water. *Annu. Rev. Fluid Mech.* **12**, 303–334. (doi:10.1146/annurev.fl.12.010180.001511)

Zakharov, V. E. 1968 Stability of periodic waves of finite amplitude on the surface of a deep fluid. *J. Appl. Mech. Tech. Phys.* **9**, 190–194. [English Translation]. (doi:10.1007/BF00913182)